Effect of shielding gas temperature on the welding fume particle formation: Theoretical model

V.I. Vishnyakov*, S.A. Kiro, M.V. Oprya, A.A. Ennan

Physical-Chemical Institute for Environment and Human Protection of Ministry of Education Science and National Academy of Sciences of Ukraine, 3 Preobrazhenska st., Odessa UA-65082, Ukraine

ABSTRACT

Inhalable particles formation in gas metal arc welding with various shielding gas temperatures is investigated by fume evolution numerical modeling. The subject of modeling is a single gas parcel of vapor-gas mixture, evolution of which under cooling based on initial temperature and vapor chemical composition is calculated. The welding fume evolution includes vapor emission from arc zone and mixing, plasma formation, nucleation, nuclei growth via material condensation and coalescence, solidification of liquid droplets and primary particles' coagulation into inhalable particles in the breathing zone. The computed results correlates well with experimental dependency of the particle sizes on the shielding gas temperature. Such a dependency is caused by the decrease of vapor-gas mixture cooling rate when the shielding gas temperature is increased, which provides the increase of particles' growth duration which leads to increase of the particle sizes.

1. Introduction

Arc welding usage is accompanied by emission of the welding materials' vapors. These vapors mix with shielding gas and air, and cool down with condensation into liquid droplets, named as the nuclei. After nuclei growth via material condensation and coalescence, these droplets are solidified and form the solid primary particles of the welding fume. Primary particles coagulation forms the inhalable particles in the breathing zone.

The numerical modeling of arc welding was intensively developed recently. All processes, such as the electric arc (Benilov, 2008), metal jointing (Islam, Buijk, Rais-Rohani, & Motoyama, 2014) and fume formation (Boselli, Colombo, Ghedini, Gherardi, & Sanibondi, 2013) are the modeling objects. Last mentioned process causes the particular interest since they are related to environmental problems. Inhalable particles have a complex chemical composition, frequently unhealthy. Therefore, welding fumes represent toxicological and ecological danger and demand attentive studying.

The high-temperature welding fume vapor is ionized via electron-atom collision and UV-radiation from arc. Therefore, nucleation and nuclei growth occur in already ionized gas, i.e. in the plasma. Many authors study the nucleation in the plasma by numerical simulation, for example: Denysenko and Azarenkov (2011); Girshick and Warthesen (2006); Shigeta, Watanabe, and Nishiyama (2004). Numerical simulation allows studying the behavior of process depending on environmental parameters and initial conditions (Murphy et al., 2009). It allows to find out what processes determine the fume formation rate (Sanibondi, 2015; Tashiro et al., 2010), also morphology and chemical composition of the welding fume particles (Carpenter, Monaghan, & Norrish, 2008).

Most of authors show chemical composition and particle generation rate of the fume in comparison with welding conditions for

---

* Corresponding author.
  E-mail addresses: dr.v.vishnyakov@gmail.com, eksvar@ukr.net (V.I. Vishnyakov).
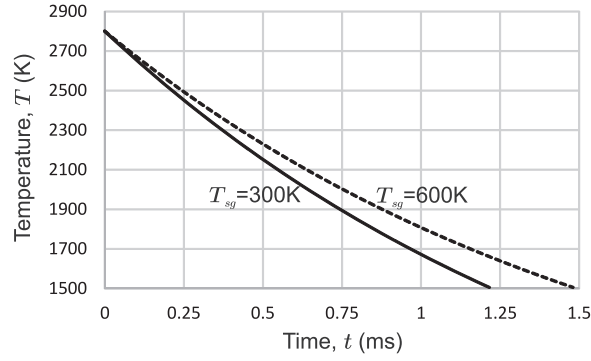
Fig. 1. Evolution of the vapor-gas mixture temperature: solid curve for T_{sg} = 300 K and dashed curve for T_{sg} = 600 K.

gas metal arc welding (GMAW) because of high utilization at various manufacturing industries in the world (Tashiro et al., 2010). The effect of shielding gas properties on the GMAW processes is also studied (Heile & Hill, 1975; Pires Quintino, & Miranda, 2007; Rao, Liao, & Tsai., 2010), in particular, the influence of shielding gas temperature on the generation of ozone was considered by Bonnet and Briand (1997).

Disperse composition of welding fume from GMAW with various shielding gas temperatures was experimentally studied by Vishnyakov, Kiro, Oprya, Ennan (2017). The vapor-gas mixture cooling rate decreases when the shielding gas temperature is increased, because the current mixture temperature is described as

$$T = T_{sg} + \left(T_0 - T_{sg}\right)\exp\frac{-t}{\tau}, \tag{1}$$

where T_0 is the initial vapor temperature; T_{sg} is the shielding gas temperature; τ is the mixing time scale, which is defined by the materials' evaporation from welding wire and molten pool, and mechanism of welding and shielding gas mixing (Villermaux & Rehab, 2000). This parameter is defined by comparison of the calculated values with experimental data, and in the system under consideration $\tau = 1.7$ ms, that has been defined by coincidence of the calculated and measured particles' chemical composition (Vishnyakov, Kiro, Oprya, Chursina, & Ennan, 2018). The evolution of the mixture temperature for two values of the shielding gas temperature is presented in Fig. 1. The change in the cooling rate should influence the nucleation and nucleus growth via condensation and coalescence.

The presented paper is devoted to numerical modeling of the primary and inhalable particles' formation in the fume from GMAW. The subject of modeling is a single gas parcel of vapor-gas mixture, which evolution under cooling based on initial temperature and vapor chemical composition is calculated. Such modeling allows describing the delicate processes during welding fume formation, in particular studying the dependency of the welding fume particle size distribution on the shielding gas temperature and comparison with experimental data (Vishnyakov et al., 2017). The simplified algorithm for calculation of primary particles' formation is presented in Appendix.

2. Description of the welding fume plasma

The vapor temperature and UV-radiation from welding arc provide ionization of atoms in the vapor-gas mixture, i.e. the system should be considered as a plasma, in which the ionization balance is described by Saha equation with taken into account photoionization (Vishnyakov, Kiro, Oprya, & Shvetz, & Ennan, 2017):

$$\frac{n_e n_i}{n_a} = \frac{\Sigma_i}{\Sigma_a}\nu_e \exp\frac{-I}{k_B T} + \frac{\pi r_a^2 j_{ph}}{\gamma_{ei}} \equiv K_S, \tag{2}$$

where n_e, n_i and n_a are the average for local thermodynamic equilibrium (LTE) region number densities of electrons, ions and atoms, respectively; $n_a = n_A - n_i$, n_A is the initial atom number density; Σ_i and Σ_a are the ion and atom statistical weights; $\nu_e = 2(m_e k_B T/2\pi\hbar^2)^{3/2}$ is the effective density of the electron states; I is the potential of atom ionization; k_B is the Boltzmann constant; T is the temperature in Kelvin; m_e is the electron mass; $\hbar$ is the Plank constant; r_a is the ionizable atom radius; γ_{ei} is the electron-ion recombination coefficient $\gamma_{ei} \sim 10^{-6}\mathrm{cm^3\,s^{-1}}$; $j_{ph} \sim 10^{16}\mathrm{cm^{-2}s^{-1}}$ is the photon flux; K_S is the Saha constant.

Electrical neutrality of the equilibrium plasma is described by the following expression:

$$n_e = n_i = n_0, \tag{3}$$

where n_0 is the unperturbed number density, which determines from Eq. (2) for multicomponent system:

$$n_0 = \sum_j \frac{K_{Sj}}{2}\left(\sqrt{1 + 4\frac{n_{Aj}}{K_{Sj}}} - 1\right), \tag{4}$$

n_{Aj} is the initial atom number density of ionizable components (without ionization), which in the vapor-gas mixture is (Vishnyakov et al., 2017)

$$n_{Aj} = \frac{P}{k_B T} \frac{g_{j0}}{\mu_j} \left[\sum \frac{g_{j0}}{\mu_j} + \frac{1}{\mu_{sg}} \frac{T_0 - T}{T - T_{sg}} \right]^{-1},$$

(5)

where P is the atmospheric pressure; g_{j0} is the initial jth component mass fraction in vapors (it is determined by the content of weld material components); μ_j is the jth component molecular mass; μ_{sg} is the shielding gas molecular mass (CO_2 in the system under consideration);

The nuclei, as the liquid particles, appear in the welding fume after nucleation. Such a system should be considered as a dusty plasma, i.e. the plasma, which contains the solid or liquid particles as a dust component (Fortov, Khrapak, Khrapak, Molotkov, & Petrov, 2004; Goree, 1994). The interphase interaction leads to the particle charging. The surface of charged particle is the additional channel for gas atoms' ionization. Therefore, there is ionization balance displacement in the space charge region (SCR) around the particle (Vishnyakov, 2005, 2006; Vishnyakov et al., 2017).

Electrical neutrality in this case is described by another expression

$$n_e - n_i = z_p n_p,$$

(6)

where n_p is the particle average number density; z_p is their average charge number (a charge in the elementary charges).

The potential distribution for particle with radius $r_p \ll r_D$ (where $r_D = \sqrt{k_B T / 8\pi e^2 n_0}$ is the screening length, and $r_D \sim 1$ μm in the system under consideration) is determined by equation:

$$\tanh \frac{r_p e\varphi(r)}{r_D k_B T} = \tanh \frac{r_p V_b}{r_D k_B T} \cdot \frac{r_p}{r} \exp \frac{r_p - r}{r_D},$$

(7)

from which follows for surface field

$$E_s = \frac{k_B T r_D}{2 e r_p^2} \sinh \frac{2 r_p V_b}{r_D k_B T}.$$

(8)

On the other hand, surface electric field from Gauss theorem is described as $E_s = e z_p / r_p^2$. Therefore, from Eq. (8) follows

$$z_p = \frac{k_B T r_D}{2 e^2} \sinh \frac{2 r_p V_b}{r_D k_B T},$$

(9)

Here should be noted, that nucleus has negative charge and potential barrier (V_b) on the particle-plasma boundary is described by following equation

$$V_b \cong \frac{2}{5} k_B T \ln \frac{n_{es}}{n_0}, \quad n_{es} < n_0,$$

(10)

where n_{es} is the surface electron number density

$$n_{es} = \nu_e \exp \frac{-W}{k_B T} + \frac{Y j_{ph}}{v_{Te}};$$

Y is the quantum yield; $v_{Te} = \sqrt{8 k_B T / \pi m_e}$ is the thermal velocity of electrons; W is the electron work function.

The calculation technique is based on evolution of the gas parcel temperature (1). Initial vapor chemical composition is determined by the welding wire (ER 70S-6): $g_{Fe} = 96.5\%$ for iron; $g_{Mn} = 2\%$ for manganese; $g_{Si} = 1\%$ for silicon; $g_{Cu} = 0.5\%$ for copper. The environmental parameters are calculated on each iteration time step by subprogram:

$$n_a, n_e, n_i, n_0, z_p, S = ENVIRONMENT\,(T, r_p, n_p, X),$$

where S is the vapor supersaturation; X is the matrix, which contains the particle component composition for multicomponent condensation.

3. Modeling of the primary particles' formation

The welding fume formation is a result of heterogeneous ion-induced nucleation in the environment enriched by the electrons. Thus, there is an exchange of energy and charges between the nucleus and the environment. Such consideration has been proposed in Refs. Vishnyakov (2008); Vishnyakov, Kiro, and Ennan (2011, 2013), where the change in Gibbs free energy ΔG as a result of nucleation is considered with taken into account the change in surface free energy as a result of the electrical double layer on the nucleus surface formation, the change in Gibbs free energy as a result of the interphase energy exchange and the change in Gibbs free energy as a result of the nucleus charging.

The two kinds of nuclei are formed by the heterogeneous ion-induced nucleation: the equilibrium nuclei with radius r_{eq}, which are in the equilibrium state with the environment; and the non-equilibrium critical nuclei with radius r_{cr}, which appear as a result of the fluctuations. The radius of the equilibrium nucleus is defined as a minimum of the function $\Delta G(r_n)$, and the radius of the critical nucleus is defined as the maximum of the function $\Delta G(r_n)$.

The number density of equilibrium nuclei with radius $r_n = r_{eq}$ is determined in the following form (Vishnyakov et al., 2013):

$$n_n = \frac{n_{a0}}{N_{an} + N_{an}^{-3/2} \exp \frac{\Delta G(r_{eq})}{k_B T}},$$

(11)

where n_{a0} is the initial (prior to the nucleation start) condensable atom number density; N_{an} is the number of atoms in one nucleus: $N_{an} = 4\pi \rho r_n^3 / 3 m_{ca}$.

The nucleation is calculated by subprogram:

$$r_{eq}, r_{cr}, n_n, N_{an}, E_{act} = NUCLEATION\,(T, n_a, n_0, S, X),$$

where all arguments except T are the matrix, and nucleus charges are calculated inside the subprogram.

The disappearance of condensable atoms should be taken into account while nucleation occurs. Thus, it is necessary to subtract the number of atoms in nuclei $n_n N_{an}$ from the equilibrium number of condensable atoms n_A. The matrix X is used for multicomponent nucleation: $n'_A = n_A - n_n N_{an} X$.

The large number density of nuclei $n_n \sim 10^{15} - 10^{16} \mathrm{cm}^{-3}$ causes their intensive Brownian collisions and coagulation, because it has thermodynamic reason (Vishnyakov & Dragan, 2003). As nuclei appear to be in the liquid state, their coagulation is a coalescence. As a result, the aggregated droplets, which grow through coalescence and condensation, are formed. However, it is necessary to take into account that the nucleation continues, and the system thermodynamics requires the presence of the nuclei with equilibrium number density (11). Therefore, number and size of nuclei cannot change via coalescence, because new nuclei appear. This requirement is removed after the nucleation termination.

Thus, already at the initial stage of nucleation the bimodal size distribution of the droplets occurs. The first mode contains the droplets of nuclei; aggregated droplets resulting from the long-term coalescence and condensation represent the second mode. It should be noted that in this case nucleation is the original "pump" for the transfer of the atoms from the gas phase into the aggregated droplets (Vishnyakov, Kiro, & Ennan, 2014a).

When droplets have grown through coalescence, they can be described by a log-normal size distribution, which is based on the number of atoms N contained in the droplets, using probability density function:

$$f_{Ni} = \frac{n_i}{N \sqrt{2\pi}\, \ln \sigma_i} \exp \frac{-(\ln N - \ln N_{0i})^2}{2 \ln^2 \sigma_i} \quad (i = 1,\ 2),$$

(12)

and the total distribution function is the superposition of these two: $f_N = f_{N1} + f_{N2}$ (Seigneur et al., 1986). Here $N_{0i} = \overline{N_i} \exp(-\ln^2 \sigma_i / 2)$ is the median of distribution; σ is the standard deviation; $\overline{N}$ is the average number of atoms in the droplets, for which the equation of the atoms conservation is as follows:

$$n_{ac} = n_n \overline{N_n} + n_{ad} \overline{N_{ad}} \equiv n_1 \overline{N_1} + n_2 \overline{N_2}.$$

The evolution of such a system can be described by the integral moments of the distribution (12) (Chan, Liu, & Chan, 2010; Estrada & Cuzzi, 2008; Whitby & McMurry, 1997). The numerical calculation of the coagulation of particles is a complex problem. Therefore, Cohen and Vaughan (1971) proposed the approximation method based on the moments of size distribution. The moments are described by the following equation:

$$M(k) = \int_0^\infty N^k f_N \, dN,$$

and the Brownian coagulation can be described by the following equation (Yu, Lin, & Chan, 2008):

$$\frac{\partial M(k)}{\partial t} = \frac{1}{2} \int_0^\infty f_N \int_0^\infty \beta\left(N, N'\right) f_{N'} [(N + N')^k - N^k - N'^k] dN' dN,$$

(13)

where N and N' are the numbers of atoms in the colliding droplets; $\beta(N, N')$ is the collision kernel. The Brownian collision kernel can be determined by the kinetic theory of gases, or by the diffusion theory according to droplet size. If the droplets are much smaller than the mean free path length of the gas molecules, the kinetic theory of gases should be used to determine the collision kernel (Shigeta et al., 2004):

$$\beta\left(N, N'\right) = \beta_0 (N^{1/3} + N'^{1/3})^2 \sqrt{\frac{N + N'}{NN'}}, \quad \beta_0 = \left(\frac{3 m_{ca}}{4\pi \rho}\right)^{1/6} \sqrt{\frac{6 k_B T}{\rho}},$$

where Coulomb interaction is neglected because $e^2 z_p z'_p / (r_p + r'_p) \ll k_B T$ (r_p is the r_n or r_{ad}; z_p is the z_n or z_{ad}, respectively).

The evolution of the moments (13) can be defined for each mode (12). As a result, the average number of atoms in the droplets of each mode is

$$\overline{N_i} = \frac{M_i(1)}{M_i(0)},$$

(14)

and the standard deviation is defined by the following equation:

$$\ln^2 \sigma_i = \ln \frac{M_i(0)M_i(2)}{M_i(1)^2}.$$

(15)

Eqs. (12)–(15) allow to describe the evolution of the coalescence in the bimodal system of droplets with taken into account both the intramodal coalescence and the intermodal association of different droplet's modes.

The coalescence is calculated by three individual subprograms:

$$n_2, \overline{N}_2, \sigma_2 = PUMP(dt, \beta_0, n_1, \overline{N}_1, \sigma_1, n_2, \overline{N}_2, \sigma_2)$$

for calculation of the coalescence at the nucleation stage;

$$n_1, \overline{N}_1, \sigma_1, n_2, \overline{N}_2, \sigma_2 = BIMODAL(dt, \beta_0, n_1, \overline{N}_1, \sigma_1, n_2, \overline{N}_2, \sigma_2)$$

for calculation of the coalescence at the nuclei growth;

$$n_1, \overline{N}_1, \sigma_1 = UNIMODAL(dt, \beta_0, n_1, \overline{N}_1, \sigma_1)$$

for calculation of the coalescence after solidification of aggregated droplets.

The last subprogram is necessary for taking into account the dependency of the solidification temperature on the droplet size (Shu et al., 2012). The droplets of the second mode (aggregated droplets) solidify earlier than the droplets of the first mode (nuclei); and the transient stage exists when the second mode is represented by solid particles, but the first mode is the liquid droplets. The bimodal coalescence terminates when the aggregated droplets become solid particles. The coalescence exists only for the first mode.

The equilibrium nucleus is in the stable stage and some activation energy is necessary for the nucleus growth $E_{act} = \Delta G(r_{cr}) - \Delta G(r_n)$. This activation energy decreases down to zero ($E_{act} \to 0$) with the vapor-gas mixture cooling, thus the equilibrium and the critical radii tend to equal value ($r_{eq} \to r_{cr}$). After that, the unrestricted growth of nuclei begins, until the condensable materials does not deplete.

The growth of nucleus with radius r_n is defined by the increment of the mass at the account of the adsorption and transpiration fluxes difference, which in the free molecular regime is described by the following equation (Fuchs, 1959; Zimmer, 2002):

$$\frac{dm_n}{dt} = \pi r_n^2 \alpha_c v_{Ta} m_{ca} \left(n_{ca} - n_{cs} \right),$$

where α_c is the evaporation–condensation coefficient (Okuyama & Zung, 1967); $v_{Ta} = \sqrt{8k_B T / \pi m_a}$ is the thermal velocity of the condensable atoms; m_{ca} is their mass; n_{ca} is their number density; n_{cs} is the number density of the condensable atoms near the nucleus surface: $n_{cs} = n_{ca} S_R / S$; S is the current supersaturation; $S_R = P_{sat}(r_n)/P_{sat}(\infty)$ is the change in vapor partial pressure at the account of the surface curvature and interphase interaction (Vishnyakov, Kiro, & Ennan, 2014b):

$$\ln S_R \cong \frac{m_{ca}}{4\pi\rho k_B T} \left[8\pi\gamma_0 \frac{r_n + 3\delta}{(r_n + 2\delta)^2} - \frac{z_n(V_b + W)}{r_n^3} - \frac{e^2(1 - z_n^2)}{2r_n^4} \right],$$

(16)

where $\gamma = \gamma_0 r_n/(r_n + 2\delta)$ is the surface free energy of the nucleus; γ_0 is the surface free energy of the flat; δ is the Tolmen length; ρ is the nucleus density.

The change in the nucleus radius as a result of growth is

$$\frac{dr_n}{dt} = \frac{1}{4\pi r_n^2 \rho} \frac{dm_n}{dt} = \frac{\alpha_c v_{Ta} m_{ca} n_{ca}}{4\rho} \left(1 - \frac{S_R}{S} \right).$$

(17)

This equation describes the nuclei growth by condensation of the predominant vapor component, i.e. the iron. However, the condensation of other components exists prior to the beginning of the basic growth.

After nucleation of the predominant component, the fluxes of the accompanying low-boiling components on to the iron nucleus appear, because the partial pressure of these components at the nucleus surface is zero. Therefore, condensation of these components on the nucleus droplet occurs, but the growth of nucleus due to iron condensation is absent. The change in the number of atoms of the jth component in the multicomponent droplet is described by the following equation (Vishnyakov et al., 2014b):

$$\frac{dN_{aj}}{dt} = \alpha_{cj} \pi r_n^2 v_{Tj} n_{aj} \left(1 - X_j \frac{S_{Rj}}{S_j} \right),$$

where X_j is the jth component fraction.

Then the change in the radius of nucleus droplet is

$$\frac{dr_n}{dt} = \sum_j \left[\frac{\alpha_{cj} v_{Tj} m_{aj} n_{aj}}{4\rho_j} \left(1 - X_j \frac{S_{Rj}}{S_j} \right) \right].$$

(18)

At the moment of nucleation the content of the accompanying low-boiling components in the nucleus $X_{j \neq Fe} = 0$. Therefore, the nucleus droplet growth due to deposition of these components on nucleus surface takes place. The growth of the nucleus or aggregated droplets via condensation of iron begins, when $r_n = r_{cr}$ or $r_{ad} = r_{cr}$.
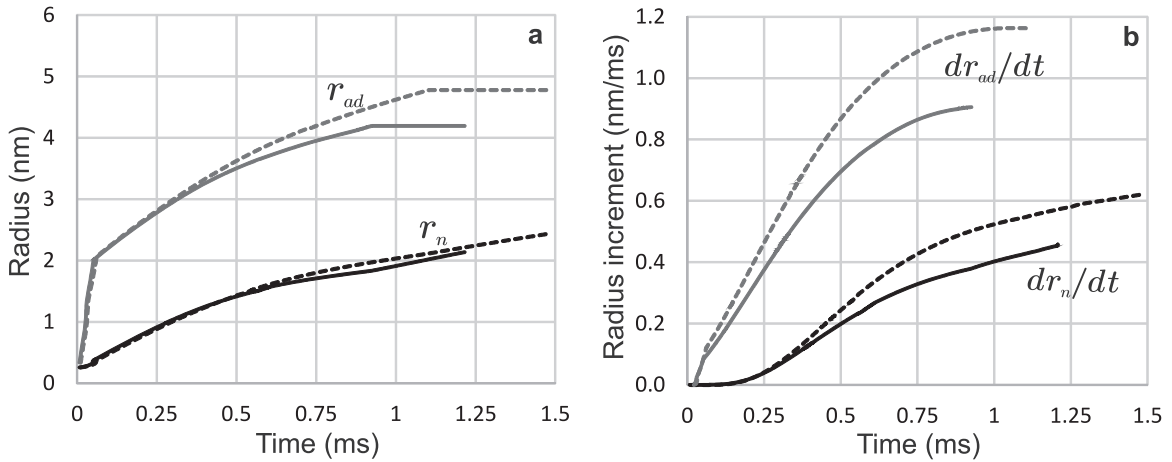
Fig. 2. Evolution of the primary particle average radii (a) and radius increments (b): solid curves for $T_{sg} = 300$ K and dashed curves for $T_{sg} = 600$ K.

The condensation growth of nuclei is calculated by subprogram:

$$dr, X = GROWTH(k, dt, T, n_a, S, r_k, z_k, V_{bk}, X),$$

where k is the particle growth type: $k = 0$ for nuclei growth when $E_{act} < k_B T$; $k = 1$ for aggregated droplets growth when $r_{ad} > r_{cr}$; $k = 2$ for condensation of low-boiling components on nuclei (iron condensation is excluded).

Evolution of the average nuclei and aggregated droplets radii with taken into account both condensation and coagulation growths is presented in Fig. 2a. In addition, evolution of radii increments by the condensation growth only (18) is presented in Fig. 2b.

Cooling of the vapor-gas mixture to the temperature of aggregated droplets solidification occurs during 0.9 ms at the shielding gas temperature of 300 K and during 1.1 ms at the shielding gas temperature of 600 K. The growth of the nucleus mode is proceeded up to 1.2 ms for $T_{sg} = 300$ K and up to 1.5 ms for $T_{sg} = 600$ K.

The solid primary particles with bimodal size distribution appear in the welding fume after solidification of nuclei and aggregated droplets (see Fig. 3). In the system under consideration, primary particles have the presented in Table 1 parameters.

4. Modeling of the inhalable particles' formation

The agglomerates generated from the solid primary particles are the irregular structures; therefore, the radius of agglomerate, which contains N primary particles (monomers), is described as

$$r_{ag} = aN^{1/D_f},$$

where a is the radius of the monomers; D_f is the fractal dimension ($D_f = 3$ for perfect sphere). In this case, the collision kernel for the free molecule regime without electrical interaction between particles is described by the following equation (Wu & Friedlander, 1992):

$$\beta\left(N, N'\right) = \beta_0 \sqrt{\frac{N + N'}{NN'}} \left(N^{1/D_f} + N'^{1/D_f}\right)^2, \quad \beta_0 = \sqrt{\frac{6k_B T a}{\rho}}, \tag{19}$$
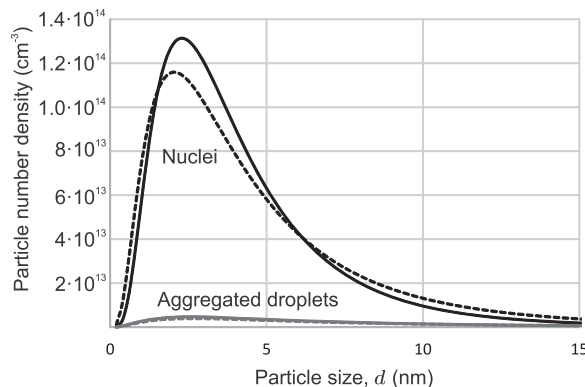

Fig. 3. Number based primary particle size distribution: solid curves for $T_{sg} = 300$ K and dashed curves for $T_{sg} = 600$ K.

Table 1

Parameters of the particle size distributions for two shielding gas temperatures.

Temperature:	300 K		600 K	
Particles:	primary	inhalable	primary	inhalable
d_1 (nm)	4.3	185	4.8	202
n_1 (cm^{-3})	$6 \cdot 10^{14}$	$3.9 \cdot 10^5$	$5.6 \cdot 10^{14}$	$3.6 \cdot 10^5$
σ_1	2.4	1.5	2.6	1.5
d_2 (nm)	8.4	209	9.5	239
n_2 (cm^{-3})	$4 \cdot 10^{13}$	$2.8 \cdot 10^4$	$3.7 \cdot 10^{13}$	$2.6 \cdot 10^4$
σ_2	2.5	1.6	2.5	1.7

where ρ is the monomer density; N and N' are the numbers of monomers in the colliding agglomerates with fractal dimension D_f.

The collision kernel for charged particles is (Vishnyakov, Kiro, Oprya, & Ennan, 2014)

$$\beta_Q\left(N, N'\right) = \beta\left(N, N'\right) \exp \frac{-U_{N,N'}}{k_B T},$$

where $U_{N,N'}$ is the interaction energy on the shortest distance between the interacting particles, which can be considered in the Coulomb approximation

$$U_{N,N'} = \frac{e^2 z_N z_{N'}}{a\left(N^{1/D_f} + N'^{1/D_f}\right)},$$

where z_N and $z_{N'}$ are the particle charge numbers, for which from Eq. (9) follows

$$z_N = \frac{k_B T r_D}{2e^2} \sinh \frac{2aN^{1/D_f} V_b}{r_D k_B T}, \tag{20}$$

and under condition $r_{ag} V_b \ll r_D k_B T$ this charge can be described as Coulomb: $z_N \cong aN^{1/D_f} V_b/e^2$.

The resulting collision kernel is

$$\beta_Q\left(N, N'\right) = \beta\left(N, N'\right) \exp \frac{-a_{N,N'} V_{bN} V_{bN'}}{e^2 k_B T}, \tag{21}$$

where $a_{N,N'} = a \cdot (NN')^{1/D_f}\left(N^{1/D_f} + N'^{1/D_f}\right)^{-1}$.

The agglomerates' coagulation leads to increase of their sizes up to values, which exceed the mean free path length and Eq. (21) becomes inapplicable. In this case the collision kernel should be described in the diffusion regime:

$$\beta_Q\left(N, N'\right) = \frac{2k_B T C(a_{N,N'})}{3\eta} \frac{a \cdot (N^{1/D_f} + N'^{1/D_f})}{a_{N,N'}} \left(1 + \frac{a_{N,N'} V_{bN} V_{bN'}}{e^2 k_B T}\right), \tag{22}$$

where η is the viscosity; $C(a)$ is the Canningham slip correction (Hagwood, Sivathanu, & Mulholland, 1999)

$$C(a) = 1 + \frac{\lambda}{a}\left(1.142 + 0.588 \exp \frac{-a}{\lambda}\right),$$

$\lambda = 67$ nm is the mean free path.

The calculation bases on the moments method with collision kernel (21) or (22) and taking into account that coagulation occurs by the both ways of collision between particles, as the intramodal and as the intermodal. The resulting inhalable particles also have the bimodal size distribution, that is correlated with experimental data by Ennan, Kiro, Oprya, and Vishnyakov (2013).

5. Discussion and comparison with experiment

The initial vapor temperature T_0 and chemical composition g_{j0}, which is determined by the composition of welding wire, and mixing time scale τ, which is determined by previous experiments (Vishnyakov et al., 2018) allow to calculate the fume evolution up to primary particles' formation. However, modeling of the primary particles' agglomeration requires the knowledge of agglomerate fractal dimension, which can be obtained via comparison with experimental data.

The measured particle size distribution in the system under consideration is presented in paper (Vishnyakov, Kiro, Oprya, Ennan et al., 2017). Search of matching between experimental data and calculations at the shielding gas temperature $T_{sg} = 300$ K leads to the fractal dimension for the first mode $D_{f1} = 1.95$ and for the second mode $D_{f2} = 2.25$. These values of the fractal dimension mean that the first mode agglomerates are the homogeneous grape-like structures, which contain mostly primary particles from nuclei; and the second mode agglomerates are closer to the heterogeneous grape-like structures, which contain both modes of the primary particles.

This assumption correlates with modeled data by Eggersdorfer and Pratsinis (2012); Sanibondi (2015), where similar particle structures are presented (See Fig. 4a and Fig. 4b); and with experimental data by Miettinen, Torvela, and Leskinen (2016), where TEM
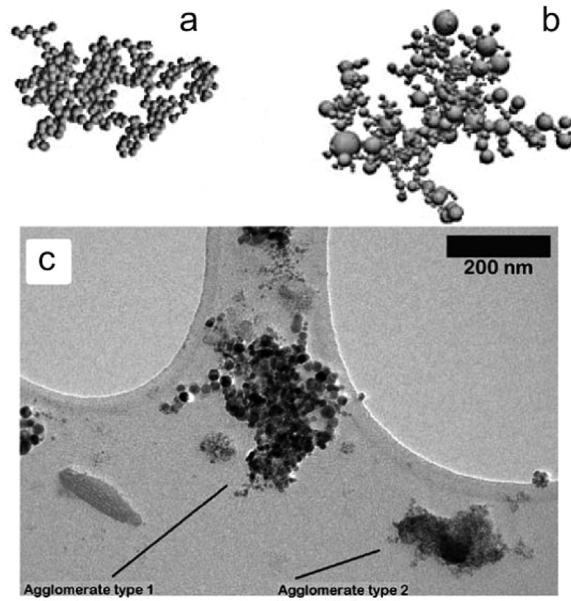
Fig. 4. Examples of probability agglomerate structures: first mode as a grape-like homoaggregate (a), second mode as a grape-like heteroaggregate (b) (Eggersdorfer & Pratsinis, 2012); TEM image of the two different agglomerate types (c) (Miettinen et al., 2016).
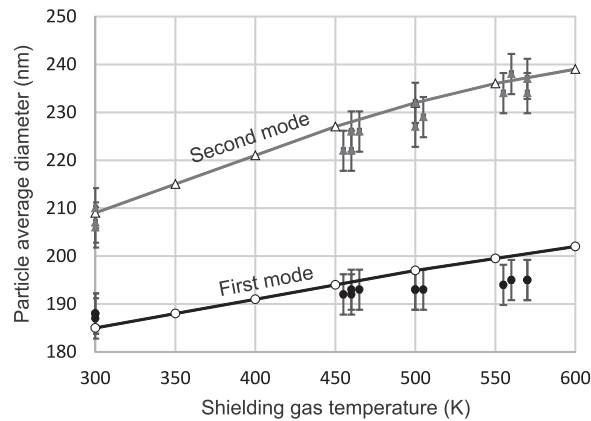

Fig. 5. Dependencies of average inhalable particle sizes on shielding gas temperature: dots are the experimental data from (Vishnyakov, Kiro, Oprya, Ennan et al., 2017); lines are the calculation results.

images are presented and the two types of agglomerates was detected. In this case, the agglomerate type 1 in Fig. 4c corresponds to the second mode of inhalable particles in the system under consideration; and the agglomerate type 2 corresponds to the first mode.

Calculating of the primary particles' formation and their coagulation gives the values, which are presented in Table 1. It should be noted that primary particles' formation occurs in the representative volume of $1 \, cm^3$. Such a volume for inhalable particles is the breathing zone about $1 \, m^3$. The inhalable particle first mode formation lasts of 0.5 ms, and this duration for the second mode is 7 ms.

The effect of shielding gas temperature on the fume formation is provided by temperature dependencies (1) and (5), because they determine the cooling rate and ionization degree. The inhalable particle average diameters calculation results with using the mentioned above initial parameters and fractal dimensions for various shielding gas temperatures are presented in Fig. 5. The shielding gas temperature influence on the particle size distribution from Vishnyakov, Kiro, Oprya, Ennan et al. (2017) experimental data is also presented in Fig. 5. The calculation results are in the measuring error limits.

6. Conclusion

Evolution of processes in the welding fume from GMAW was investigated via numerical modeling. It allows defining the primary particles' size distribution and inhalable particles' morphology and size distribution. Both primary and inhalable particles have the bimodal size distribution. Number density of the primary particles of smaller mode ($\sim 4 \, nm$) greatly exceeds the large mode ($\sim 8 \, nm$) number density.

Search of matching between calculation results and experimental data allows defining the inhalable particles' fractal dimensions. Apparently, the first inhalable particle mode can be identified as the grape-like homoaggregates; and the second mode – as the grape-like heteroaggregates. Different types of agglomerates contain different numbers and types of the primary particles that reflects their formation mechanism.

The calculated results correlates well with experimental dependency of the particle sizes on the shielding gas temperature (Vishnyakov et al., 2017). Such a dependency is caused by the decrease of vapor-gas mixture cooling rate when the shielding gas temperature is increased. Therefore, duration of the particles' growth via vapor condensation and coalescence is increased, what leads to increase of the particle sizes.

Appendix. Algorithm for calculation of primary particles' formation

Algorithm 1.

$T_0 = 2800$ K; $T_{sg} = 300$ K, or another value;

$\tau = 1.7$ ms; $dt = 1$ μs; $r_p = 0$; $n_p = 0$; $t = 0$; $X = [1\,0\,0\,0]$;

$NUCL = 1$

T_{s1} and T_{s2} are the solidification temperatures for nuclei and aggregated droplets, respectively.

while $T > T_{s1}$ **do**

    $t \leftarrow t + dt$

    $T \leftarrow T_{sg} + (T_0 - T_{sg}) \cdot \exp(-t/\tau)$

    $n_a, n_e, n_i, n_0, z_p, S \leftarrow ENVIRONMENT(T, r_p, n_p, X)$

    if $NUCL = 1$ **then**

        $r_n, r_{cr}, n_n, N_{an}, E_{act} \leftarrow NUCLEATION(T, n_a, n_0, S, X)$

        if $r_n > 0$ **then**

            $dr, X \leftarrow GROWTH(2, dt, T, n_a, S, r_n, z_n, V_{bn}, X)$

            $r_n \leftarrow r_n + dr$

            $n_{ad}, \bar{N}_{ad}, \sigma_{ad} \leftarrow PUMP(dt, \beta_0, n_1, \bar{N}_1, \sigma_1, n_2, \bar{N}_2, \sigma_2)$

            $r_{ad} \leftarrow (3m_{ca}\bar{N}_{ad}/4\pi\rho)^{1/3}$

            if $r_{ad} \geq r_{cr}$ **then**

                $dr, X \leftarrow GROWTH(1, dt, T, n_a, S, r_{ad}, z_{ad}, V_{bad}, X)$

                $r_{ad} \leftarrow r_{ad} + dr$

             end

            if $r_n \geq r_{cr}$ **then**

                $NUCL \leftarrow 0$

            end

        end

    else

        $dr, X \leftarrow GROWTH(0, dt, T, n_a, S, r_n, z_n, V_{bn}, X)$

        $r_n \leftarrow r_n + dr$

        if $T > T_{s2}$ **then**

            $dr, X \leftarrow GROWTH(1, dt, T, n_a, S, r_{ad}, z_{ad}, V_{bad}, X)$

            $r_{ad} \leftarrow r_{ad} + dr$

            $n_n, \bar{N}_n, \sigma_n, n_{ad}, \bar{N}_{ad}, \sigma_{ad} \leftarrow BIMODAL(dt, \beta_0, n_n, \bar{N}_n, \sigma_n, n_{ad}, \bar{N}_{ad}, \sigma_{ad})$

            $r_n \leftarrow (3m_{ca}\bar{N}_n/4\pi\rho)^{1/3}$

            $r_{ad} \leftarrow (3m_{ca}\bar{N}_{ad}/4\pi\rho)^{1/3}$

        else

            $n_n, \bar{N}_n, \sigma_n \leftarrow UNIMODAL(dt, \beta_0, n_n, \bar{N}_n, \sigma_n)$

            $r_n \leftarrow (3m_{ca}\bar{N}_n/4\pi\rho)^{1/3}$

        end

    end

end

References

Benilov, M. S. (2008). Understanding and modelling plasma-electrode interaction in high-pressure arc discharges: A review. *Journal of Physics D: Applied Physics, 41*, 144001.

Bonnet, Ch., Briand, F., Suzon, S., & Lefebvre, Ph. (1997). Process and apparatus for reducing the emission of ozone produced during a gas shielded arc welding operation. Patent: EP0799666A1.

Boselli, M., Colombo, V., Ghedini, E., Gherardi, M., & Sanibondi, P. (2013). Two-dimensional time-depended modelling of fume formation in a pulsed gas metal arc welding process. *Journal of Physics D: Applied Physics, 46*, 224006.

Carpenter, K. R., Monaghan, B. J., & Norrish, J. (2008). Influence of shielding gas on fume size morphology and particle composition for gas metal arc welding. *The Iron and Steel Institute of Japan International, 48*, 1570–1576.

Chan, T. L., Liu, Y. H., & Chan, C. K. (2010). Direct quadrature method of moments for the exhaust particle formation and evolution in the wake of the studied ground vehicle. *Journal of Aerosol Science, 41*, 553–568.

Cohen, E. R., & Vaughan, E. U. (1971). Approximate solution of the equations for aerosol agglomeration. *Journal of Colloid and Interface Science, 35*, 612–623.

Denysenko, I., & Azarenkov, N. A. (2011). Formation of vertically aligned carbon nanostructures in plasmas: Numerical modelling of growth and energy exchange. *Journal of Physics D: Applied Physics, 44*, 174031.

Eggersdorfer, M. L., & Pratsinis, S. E. (2012). The structures of agglomerates consisting of polydisperse particles. *Aerosol Science and Technology, 46*, 347–353.

Ennan, A. A., Kiro, S. A., Oprya, M. V., & Vishnyakov, V. I. (2013). Particle size distribution of welding fume and its dependency on conditions of shielded metal arc welding. *Journal of Aerosol Science, 64*, 103–110.

Estrada, P. R., & Cuzzi, J. N. (2008). Solving the coagulation equation by the moments method. *The Astrophysical Journal, 682*, 515–526.

Fortov, V. E., Khrapak, A. G., Khrapak, S. A., Molotkov, V. I., & Petrov, O. F. (2004). Dusty plasmas. *Physics-Uspekhi, 47*, 447–492.

Fuchs, N. A. (1959). In R. S. Bradley (Ed.). *Evaporation and Droplet Growth in Gaseous Media*(1st Edition). New York: Pergamon Press ISBN: 9781483225630.

Girshick, S. L., & Warthesen, S. J. (2006). Nanoparticles and plasmas. *Pure and Applied Chemistry, 78*, 1109–1116.

Goree, J. (1994). Charging of particles in plasma. *Plasma Sources Science and Technology, 3*, 400–406.

Hagwood, C., Sivathanu, Y., & Mulholland, G. (1999). The DMA transfer function with Brownian motion a trajectory/Monte-Carlo approach. *Aerosol Science and Technology, 30*, 40–61.

Heile, R. F., & Hill, D. C. (1975). Particle fume generation in arc welding processes. *Welding Journal Research Supplement, 54*, 201s–210s.

Islam, M., Buijk, A., Rais-Rohani, M., & Motoyama, K. (2014). Simulation-based numerical optimization of arc welding process for reduced distortion in welded structures. *Finite Elements in Analysis and Design, 84*, 54–64.

Miettinen, M., Torvela, T., & Leskinen, J. T. T. (2016). Physicochemical characterization of aerosol generated in gas tungsten arc welding of stainless steel. *Annals of Occupational Hygiene, 60*, 960–968.

Murphy, A. B., Tanaka, M., Yamamoto, K., Tashiro, S., Sato, T., & Lowke, J. J. (2009). Modelling of thermal plasmas for arc welding: The role of the shielding gas properties and of metal vapour. *Journal of Physics D: Applied Physics, 42*, 194006.

Okuyama, M., & Zung, J. T. (1967). Evaporation-condensation coefficient for small droplets. *Journal of Chemical Physics, 46*, 1580–1585.

Pires, I., Quintino, L., & Miranda, R. M. (2007). Analysis of the influence of shielding gas mixtures on the gas metal arc welding metal transfer modes and fume formation rate. *Materials and Design, 28*, 1623–1631.

Rao, Z. H., Liao, S. M., & Tsai, H. L. (2010). Effect of shielding gas compositions on arc plasmas and metal transfer in gas metal arc welding. *Journal of Applied Physics, 107*, 044902.

Sanibondi, P. (2015). Numerical investigation of the effects of iron oxidation reactions on the fume formation mechanism in arc welding. *Journal of Physics D: Applied Physics, 48*, 345202.

Seigneur, C., Hudischewskyj, A. B., Seinfeld, J. H., Whitby, K. T., Whitby, E. R., Brock, J. R., & Barnes, H. M. (1986). Simulation of aerosol dynamics: A comparative review of mathematical models. *Aerosol Science and Technology, 5*, 205–222.

Shigeta, M., Watanabe, T., & Nishiyama, H. (2004). Numerical investigation for nano-particle synthesis in an RF inductively coupled plasma. *Thin Solid Films, 457*, 192–200.

Shu, Q., Yang, Y., Zhai, Y., Sun, D. M., Xiang, H. J., & Gong, X. G. (2012). Size-dependent melting behavior of iron nanoparticles by replica exchange molecular dynamics. *Nanoscale, 4*, 6307–6311.

Tashiro, S., Zeniya, T., Yamamoto, K., Tanaka, M., Nakata, K., Murphy, A. B., ... Suzuki, K. (2010). Numerical analysis of fume formation mechanism in arc welding. *Journal of Physics D: Applied Physics, 43*, 434012.

Villermaux, E., & Rehab, H. (2000). Mixing in coaxial jets. *Journal of Fluid Mechanics, 425*, 161–185.

Vishnyakov, V. I., & Dragan, G. S. (2003). Thermodynamic reasons of agglomeration of dust particles in the thermal dusty plasma. *Condensed Matter Physics, 6*, 687–692.

Vishnyakov, V. I. (2005). Interaction of dust grains in strong collision plasmas: Diffusion pressure of nonequilibrium charge carriers. *Physics of Plasmas, 12*, 103502.

Vishnyakov, V. I. (2006). Electron and ion number densities in the space charge layer in thermal plasmas. *Physics of Plasmas, 13*, 033507.

Vishnyakov, V. I. (2008). Homogeneous nucleation in thermal dust-electron plasmas. *Physical Review E, 78*, 056406.

Vishnyakov, V. I., Kiro, S. A., & Ennan, A. A. (2011). Heterogeneous ion-induced nucleation in thermal dusty plasmas. *Journal of Physics D: Applied Physics, 44*, 215201.

Vishnyakov, V. I., Kiro, S. A., & Ennan, A. A. (2013). Formation of primary particles in welding fume. *Journal of Aerosol Science, 58*, 9–16.

Vishnyakov, V. I., Kiro, S. A., & Ennan, A. A. (2014aa). Bimodal size distribution of primary particles in the plasma of welding fume: Coalescence of nuclei. *Journal of Aerosol Science, 67*, 13–20.

Vishnyakov, V. I., Kiro, S. A., & Ennan, A. A. (2014bb). Multicomponent condensation in the plasma of welding fumes. *Journal of Aerosol Science, 74*, 1–10.

Vishnyakov, V. I., Kiro, S. A., Oprya, M. V., & Ennan, A. A. (2014c). Coagulation of charged particles in self-organizing thermal plasmas of welding fumes. *Journal of Aerosol Science, 76*, 138–147.

Vishnyakov, V. I., Kiro, S. A., Oprya, M. V., Shvets, O. I., & Ennan, A. A. (2017a). Nonequilibrium ionization of welding fume plasmas; Effect of potassium additional agent on the particle formation. *Journal of Aerosol Science, 113*, 178–188.

Vishnyakov, V. I., Kiro, S. A., Oprya, M. V., & Ennan, A. A. (2017b). Effects of shielding gas temperature and flow rate on the welding fume particle size distribution. *Journal of Aerosol Science, 114*, 55–61.

Vishnyakov, V. I., Kiro, S. A., Oprya, M. V., Chursina, O. D., & Ennan, A. A. (2018). Numerical and experimental study of the fume chemical composition in gas metal arc welding. *Aerosol Sci. Eng.*. https://doi.org/10.1007/s41810-018-0028-2.

Whitby, E. R., & McMurry, P. H. (1997). Modal aerosol dynamics modeling. *Aerosol Science and Technology, 27*, 673–688.

Wu, M. K., & Friedlander, S. K. (1992). Enhanced power law agglomerate growth in the free molecule regime. *Journal of Aerosol Science, 24*, 273–282.

Yu, M., Lin, J., & Chan, T. (2008). A new moment method for solving the coagulation equation for particles in brownian motion. *Aerosol Science and Technology, 42*, 705–713.

Zimmer, A. T. (2002). The influence of metallurgy on the formation of welding aerosols. *Journal of Environmental Monitoring, 4*, 628–632.